Title
Allosteric Inhibition of the Epidermal Growth Factor Receptor

Authors
Sinclair, Julie KL
Robertson, Wesley E
Mozumdar, Deepto
et al.

Peer reviewed

Allosteric Inhibition of the Epidermal Growth Factor Receptor

Julie K.L. Sinclair[1], **Wesley E. Robertson**[2], **Kim Quach**[1], **Deepto Mozumdar**[1,3], **Alanna Schepartz**[3,4,*]

[1]Department of Chemistry, Yale University, New Haven, CT 06520

[2]Molecular, Cellular, and Developmental Biology, Yale University, New Haven, CT 06520

[3]Department of Chemistry, University of California, Berkeley, CA 94705

[4]Department of Molecular and Cell Biology, University of California, Berkeley, CA 94705

Abstract

We previously reported a family of hydrocarbon-stapled peptides designed to interact with the EGFR juxtamembrane (JM) segment, blocking its ability to form a coiled coil dimer that is essential for receptor activation. These hydrocarbon-stapled peptides, most notably E1[S], decreased the proliferation of cell lines that express wild type EGFR (H2030 and A431) as well as those expressing the oncogenic mutants EGFR L858R (H3255) or L858R/T790M (H1975). Although our previous investigations provided evidence that E1[S] interacted with EGFR directly, the location and details of these interactions were not established. Here we apply biochemical and cross-linking mass spectrometry tools to define the interactions between E1[S] and EGFR that result in EGFR inhibition. Our results suggest that E1[S] interacts simultaneously with both the JM and C-lobe of the activator kinase, effectively displacing the JM of the receiver kinase. This model suggests that E1[S] inhibits EGFR by both mimicking and inhibiting JM coiled coil formation and suggests a novel strategy for the design of allosteric EGFR inhibitors.

Graphical Abstract
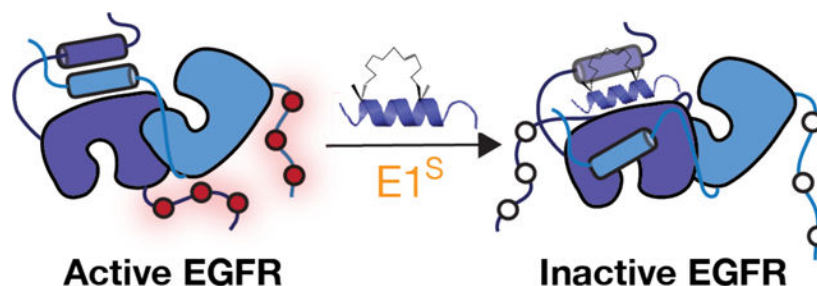
Keywords

receptor tyrosine kinase; coiled coil; information transfer; oncogene

INTRODUCTION

The epidermal growth factor receptor (EGFR)[1–5] is a receptor tyrosine kinase that acts as a conduit for information flow across the plasma membrane. In normal cells, EGFR communicates signals that regulate key events in the coordination of cell growth, differentiation, and migration.[6] Misregulation of this information flow, by virtue of EGFR mutation or over-expression, is associated with many human cancers.[7–10]

EGFR is inhibited clinically by both monoclonal antibodies and small molecules.[11,10,12,13] Clinically approved monoclonal antibodies such as cetuximab,[14–16] panitumumab (ABX-EGF/E7.6.3),[17,18] nimotuzumab (h-R3),[19] and necitumumab[20,21] bind directly to the EGFR extracellular domain (ECD) to competitively inhibit the binding of growth factors required for receptor activation. By contrast, small molecule inhibitors of EGFR are tyrosine kinase inhibitors (TKIs) that compete directly or indirectly with the binding of ATP to the intracellular kinase domain.[22,23] First generation TKIs such as erlotinib (OSI-774)[24,25] and gefitinib (ZD1839/Iressa) [26,27] target a constitutively active, oncogenic EGFR variant (L858R-EGFR)[28–30] that accounts for nearly 7–8% of all EGFR mutations found in patient populations[31–33] by competing reversibly with ATP. Second and third generation TKIs such as afatinib (BIBW-2992)[34,35], rociletinib (CO-1686),[36,35] WZ-4002[37] and osimertinib (AZD-9291)[38–40] target a more drug-resistant variant L858R/T790M-EGFR[33] by irreversibly alkylating a conserved active site cysteine side chain (C797). Monoclonal antibodies and small molecules that interact directly with EGFR can also be engineered to induce EGFR degradation via either proteasomal[41–47] or lysosomal[48] pathways.

EGFR activity can also be inhibited allosterically. Small molecule allosteric inhibitors such as EAI045[49] and JBJ-04–125-02[50] inhibit the kinase activity of oncogenic EGFR variants (most notably L858R/T790M/C797S EGFR[51]) by binding to an allosteric pocket located within the kinase domain. In addition, there are now several reports[52–58] of peptide or peptidomimetic inhibitors that target the JM segment, an intracellular region whose dimerization is essential for kinase activation.[59–63] One set of inhibitors are hydrocarbon stapled peptides[64–66] designed to inhibit EGFR by blocking the formation of the antiparallel JM coiled coil dimer (Figure 1).[54,55]

The most active hydrocarbon-stapled peptide evaluated was E1[S] (Figure 1), which contains residues 650–666 of the EGFR JM segment with residues 654 and 661 substituted with (R)-2-(7-octenyl)alanine and (S)-2-(4-pentenyl)-alanine,[54,64] respectively, to install an *i,i+7* hydrocarbon cross-link between residues 5 and 12. E1[S] decreased the proliferation of cell lines that express wild type EGFR (A431, H2030),[3,54,67] as well as those expressing the oncogenic mutants EGFR L858R (H3255) or L858R/T790M (H1975).[54,67] E1[S] also effectively down-regulated the autophosphorylation of both EGFR and downstream activators such as Akt and Erk in A431 cells.[55]

Multiple lines of evidence provided support for a direct physical association between EGFR and E1[S]. An E1[S] analog modified with an N-terminal biotin ([B]E1[S]) sequestered full-length EGFR from CHO-K1 cell lysates, providing support for a direct physical association between E1[S] and EGFR.[54] Additional evidence for a direct interaction between E1[S] and the EGFR JM derived from bipartite tetracysteine display experiments,[68,61–63] which revealed that E1[S] inhibited the formation of both EGF-type and TGF-α-type JM coiled-coils whereas inactive variants such as T1[S] had no effect (Figure S1B,C).[54]

While our previous work[54,55] provided solid evidence that E1[S] interacts directly with EGFR to inhibit its tyrosine kinase activity, the precise location of this interaction was not established. While the simplest interpretation of our previous data[54,55] supports a direct interaction between E1[S] and the EGFR JM, we could not rule out an alternative model in which either E1[S] interacts with EGFR elsewhere and allosterically inhibits coiled coil formation, or more complex models in which E1[S] interacts with more than one region of the 1186-amino acid receptor. In this work, we apply biochemical and cross-linking mass spectrometry tools to identify the complex interactions between E1[S] and EGFR that result in tyrosine kinase inhibition. Our results are consistent with a model in which E1[S] interacts simultaneously with both the JM segment and the C-lobe of the activator kinase, displacing the JM of the receiver kinase. This model suggests that the inhibition of EGFR kinase activity by E1[S] arises not only from inhibiting coiled coil formation but also by blocking an essential intramolecular interaction between the C-terminus of the JM (the region commonly referred to as the 'JM latch'[60]) with the kinase lobe. These types of interactions could form the basis for a novel family of allosteric EGFR inhibitors.

MATERIALS AND METHODS

Materials.

All materials used in this study are described in the Supporting Information document.

Peptide Synthesis and Characterization.

Peptide synthesis, reverse-phase HPLC purification, MS confirmation, CD structural determination, as well as profiling by cell viability, immuno-blot analysis of EGFR phospho-inhibition, and bipartite tetracysteine display (ReAsH labeling) assays are described in the Supplemental Experimental Procedures.

Lysate pull-down and cross-linking.

A431 cells or CHO-K1 cells (transiently transfected with WT EGFR, EGFR-GGS, EGFR1–998, or EGFR 958–1029 with the TransitCHO transfection kit, Mirus Bio, according to directions) were harvested by using a non-enzymatic cell dissociation solution (Sigma), separated into aliquots containing 1×10^6 cells, and lysed on ice for 1–2 h with 100 μL Lysis Buffer (50 mM Tris (pH 7.5), 150 mM NaCl, 1 mM EDTA, 1 mM NaF, 1% Triton X-100,) that was supplemented with protease and phosphatase inhibitor cocktails (Roche). Clarified lysates were then treated with 25 μM affinity probe peptides (^{B}JM^{WT}, ^{B}E1^S, ^{B}E1 $_L^S$, BT1^S, ^{B}E4^S, ^{DB}E1^S, ^{BD}E1^S, ^{DB}E4^S, or ^{BD}E4^S) in 300 μL of binding buffer (50 mM Tris, 150 mM NaCl, pH 7.5), incubated with constant rotation for 2 h at 4°C, and then incubated for 10 min on ice with or without UV irradiation (365 nm, UVL-56 handheld UV Lamp, 6W). Streptavidin-coated magnetic beads (100 μL slurry, GE Healthcare Biosciences) were added to each reaction and incubated with constant rotation for 16 h at 4°C. Beads were then washed with washing buffer (50 mM Tris, 150 mM NaCl, 2 M urea, pH 7.5) three times, as previously described.[54] To elute the sequestered proteins, the washed beads were then incubated with 100 μL elution buffer (2% SDS) at 95°C for 10 min. Eluted proteins were then incubated with protein-loading buffer and resolved by SDS-PAGE analysis, using 10% polyacrylamide gels (BioRad), followed by staining with Silver Stain Plus (BioRad) or transfer to PVDF membranes for immuno-blotting (iBlot apparatus, Invitrogen). Immuno-blotting was performed as previously described [54] by utilizing rabbit anti-EGFR, anti-Biotin, and anti-FLAG primary antibodies, followed by an HRP-conjugated anti-rabbit secondary antibody (Cell Signaling Technology). Blots were visualized using Clarity Western ECL reagents.

Photo-cross-linking assays with purified EGFR fragments.

Purified EGFR fragments (EGFR645–1186, EGFR672–1186, and EGFR1–621; Sigma-Aldrich) were diluted into 100 μL of binding buffer (50 mM Tris, 150 mM NaCl, pH 7.5) and incubated with indicated equivalents of photo-affinity stapled peptide analogs, with rotation for 2 h at 4°C in the dark. The samples were then irradiated with a 365 nm UV lamp (365 nm, UVL-56 handheld UV Lamp, 6W) for 10 min on ice. Proteins were then prepared for LC-MS/MS analysis or incubated with gel-loading dye and subjected to SDS-PAGE analysis (10% polyacrylamide gel). Gels were then either stained with Silver Stain Plus (BioRad) or transferred to PVDF membranes (iBlot membranes, Invitrogen) for subsequent immuno-blotting, as previously described [54], by utilizing a rabbit anti- Biotin primary antibody, followed by a HRP-conjugated anti-rabbit secondary antibody (Cell Signaling Technology). Blots were visualized using Clarity Western ECL reagents.

In-Solution trypsin digest of protein samples.

EGFR645–1186 protein samples, post photo-cross-linking assay, were reduced with 10 mM dithiothreitol (DTT) for 1 h at room temperature, followed by carbamidomethylation with 15 mM iodoacetamide (IAA) for 30 min at room temperature (in the dark). Protein samples were then precipitated, by adding a 50/50 methanol/acetone mix in a 4:1 v:v ratio to the sample, which was then incubated overnight at − 80°C. Chilled protein samples were centrifuged for 30 min at $16,000 \times g$ at 4°C, from which the resulting pellet was isolated

for subsequent trypsinization. Trypsin digest was performed by resuspending the protein pellet in 50 mM ammonium bicarbonate buffer (100 μL), to which Trypsin/LysC (Promega Corporation) was added in a 1:20 w:w ratio to the sample. The protein trypsin digested at 37°C for 6 h, then quenched with 10 μL of 5% formic acid. Trypsinized peptides were then extracted by SpeedVac-ing the tryptic solution. Dried peptides were resuspended in 0.1% formic acid (20 μL), then desalted, concentrated, and purified with a C18 Resin Zip Tip (EMD Millipore).

LC-MS/MS analysis of tryptic EGFR645–1186 peptides.

LC-MS/MS processing was performed by the Yale MS & Proteomics Resource of the Keck Biotechnology Resource Laboratory (New Haven, CT). After ZipTip desalting, the peptide sample was SpeedVac-ed dry and dissolved in 2% Formic Acid/0.1% Trifluoroacetic Acid. An estimated 125 ng was injected for LC-MS/MS analysis on a Thermo Scientific Q Exactive Plus mass spectrometer equipped with a Waters nanoAcquity UPLC system utilizing a binary solvent system (Buffer A: 100% water, 0.1% formic acid; Buffer B: 100% acetonitrile, 0.1% formic acid). Trapping was performed at 5 μl/min, 97% Buffer A for 3 min using a Waters Symmetry® C18 180 μm x 20 mm trap column. Peptides were separated using an ACQUITY UPLC PST (BEH) C18 nanoAcquity Column 1.7 μm, 75 μm x 250 mm (37°C) and eluted at 330 nL/min with the following gradient: 3% buffer B at initial conditions; 5% B at 1 minute; 30% B at 140 minutes; 50% B at 155 minutes; 90% B at 160–170 min; return to initial conditions at 171 minutes. MS was acquired in profile mode over the 300–1,500 m/z range using 1 microscan, 70,000 resolution, AGC target of 3E6, and a full max ion time of 45 ms. Data dependent MS/MS were acquired in centroid mode using 1 microscan, 17,500 resolution, AGC target of 1E5, full max IT of 100 ms, 1.7 m/z isolation window, and a normalized collision energy of 28. Up to 20 MS/MS were collected per MS scan on species with an intensity threshold of 1E4, charge states 2–6, peptide match preferred, and dynamic exclusion set to 20 seconds.

Protein identification and sequence coverage confirmation with MyriMatch/BumberDash and ID Picker.

Mascot generic format (mgf) files, obtained from LC-MS/MS analysis on an Orbitrap Q Exactive mass spectrometer at the Yale Keck Mass Spectrometry Facility (New Haven, CT), were further analyzed using the MyriMatch/BumberDash (v.1.4.115) and ID Picker (v.2.6.271.0) software suite [69]. A FASTA protein sequence database of the human proteome (UniProt/SwissProt) was utilized as a reference, supplemented with the manual addition of the GST-tagged EGFR645–1186 protein sequence. Tandem mass spectra were matched with a mass tolerance of 25 ppm on precursor masses and 75 ppm for fragment ions. Tryptic peptide matches were considered with up to five missed Lys/Arg cleavage sites (and an inhibition of cleavage when the site precedes Pro) along with the static modification carbamidomethylation of Cysteine (+57.0214 amu) and the variable modification oxidation of Methionine (+15.99 amu). A false-detection rate (FDR) of 5%, with a minimal peptide length of five amino acids, was set.

StavroX cross-linking site identification.

Assignment of EGFR645–1186 residues that were cross-linked by photo-affinity stapled peptide analogs ($^{DB}E1^S$, $^{BD}E1^S$, $^{DB}E4^S$, or $^{BD}E4^S$) was performed with StavroX (version 3.6.0).[70] StavroX in-silico cross-linked peptide fragments, calculated by generating a tryptic peptide library derived from a FASTA file containing the amino acid sequence of EGFR645–1186 (SRP 0239, Sigma) and the photo-affinity stapled peptide analog ($^{DB}E1^S$, $^{BD}E1^S$, $^{DB}E4^S$, or $^{BD}E4^S$), were compared against the MS and MS/MS data extracted from Mascot generic format (mgf) files that were obtained from LC-MS/MS analysis on an Orbitrap Q Exactive mass spectrometer at the Yale Keck Mass Spectrometry Facility (New Haven, CT). A maximum mass deviation of 10 ppm was applied between theoretical and experimental precursor and fragment ions. Only b- and y-type ions with a signal-to-noise ratio (S/N) 2 were considered for comparison with theoretical fragment ion masses. All amino acids were defined as potential cross-linking sites for the Diazirine(SDA)-labeled N-terminal Lysine residue of $^{DB}E1^S$ and $^{DB}E4^S$, or for the Diazirine(SDA)-labeled C-terminal Lysine residue of BDE1^S and $^{BD}E4^S$. Carbamidomethylation of Cysteine (+57.0214 amu), oxidation of Methionine (+15.99 amu), and three missed trypsin cleavage sites for Lysine and Arginine were considered. Candidate cross-link sites with high scores (lower than the false-detection rate (FDR) of 5%, based upon the distribution of false-positives derived from the reverse protein sequences) were manually evaluated before being assigned as positives. The manual evaluation involved confirming the presence and abundance of b- and y-type fragment ions that were used to identify the cross-linked peptide adducts.

RESULTS

The interaction of EGFR with E1^S demands an intact, native sequence JM segment.

First, we sought to determine whether the interactions of E1^S with EGFR demanded the presence of an intact, native sequence JM segment. These experiments made use of a previously reported EGFR variant, EGFR-GGS,[71] in which ten consecutive copies of the tripeptide Gly-Gly-Ser replace residues 650–680 of EGFR (virtually the entire JM segment) (Figure 2A). EGFR-GGS can be expressed in CHO-K1 cells at levels comparable to WT EGFR[71] and undergoes growth factor-induced dimerization, but the kinase remains inactive (Figure 2B) - no autophosphorylation can be detected.[71] We hypothesized that if a native JM sequence is necessary for E1^S to bind EGFR, then a biotinylated analog of E1^S (^{B}E1^S)[54] should interact more favorably with WT EGFR than with EGFR-GGS, and thereby sequester more EGFR from CHO-K1 cell lysates in traditional pull-down assays. As negative controls, we prepared biotinylated analogs of the native WT JM sequence (^{B}JM^{WT}) and two additional negative controls: hydrocarbon-stapled analogs of E1^S in which the three leucine residues (L655, L658 and L659) that contribute to EGF-type coiled coil formation [60–62] are replaced by alanine (^{B}E1 $_L$S)[54] and one (^{B}T1^S) in which the hydrocarbon staple replaces leucine residues (L655 and L659)[54] (Figure 1, Table S1). Individually, these three peptides, unadorned by a biotin tag and present at concentrations as high as 10 μM, fail to detectably inhibit EGFR activity in A431 cells (Figure S1A).[54]

We first confirmed that EGFR-GGS was expressed at levels comparable to WT EGFR in transiently transfected CHO-K1 cells[71] (Figure 2C). Next, we prepared lysates from

CHO-K1 cells transiently transfected with plasmids encoding WT EGFR or EGFR-GGS, treated the lysates for 2h at 4°C with [B]E1[S] (0–25 μM) (Figure 2D) or the biotinylated analogs ([B]JM[WT], [B]E1 [L]S and [B]T1[S]; 25 μM) (Figure 2E) and isolated the interacting proteins using streptavidin-conjugated magnetic beads. The eluted proteins were resolved by SDS PAGE and the relative levels of sequestered WT EGFR or EGFR-GGS evaluated by immunoblotting with an anti- EGFR antibody (Figure 2D and E). We observed that although both WT EGFR and EGFR-GGS were sequestered by [B]E1[S] from CHO-K1 cell lysates in a concentration-dependent manner (Figure 2D), at a given concentration of [B]E1[S], the level of WT EGFR sequestered from cell lysates was approximately 3-fold higher than the level of EGFR-GGS (Figure 2D and E). In contrast, the levels of both WT-EGFR and EGFR-GGS sequestered by the negative controls BJM[WT] and [B]T1[S] (25 μM) was negligible, providing evidence that the sequestration by [B]E1[S] required both the induced secondary structure provided by the hydrocarbon staple and a specific interaction with the receptor (Figure 2E). Interestingly with the negative control [B]E1 [L]S (25 μM), although WT EGFR was sequestered 2-fold less than by [B]E1[S], comparable amounts of EGFR-GGS were sequestered by equal concentrations of [B]E1 [L]S and [B]E1[S] (Figure 2E). These results suggest that E1[S] and E1 [L]S contain residues that bind the JM segment of EGFR, regardless of the JM sequence, or that they also bind another region of EGFR *(vide infra)*.

Photo-affinity labeling experiments confirm that an intact, native sequence JM segment is required for interaction between E1[S] and EGFR.

We next designed a set of photo-affinity probes to more directly localize the E1[S] interaction site within EGFR. These probes ([DB]E1[S] and BDE1[S]) contained the complete sequence of E1[S], extended at both the N- and C-terminus to include either a biotin tag (installed using NHS-LC-biotin) or a methyl diazirine tag (installed using NHS-diazirine, succinimidyl 4,4'-azipentanoate)[72,73] (Figure 3A, Table S1). Irradiation of a diazirine with 330–370 nm light induces loss of N_2 and formation of a carbene that can insert into proximal C-H, N-H, and O-H bonds.[74] When the diazirine is appended to a protein-binding ligand, this insertion reaction can facilitate the identification of amino acids that are proximal to the ligand interaction site.[72] As negative controls, we prepared an analogous set of biotinylated and photo-affinity probes ([B]E4[S], [DB]E4[S] and [BD]E4[S]; Table S1) containing the sequence of E4[S], an inactive variant of E1[S] that inhibits neither EGFR activity nor JM coiled-coil formation (Figure S1).[54] Preliminary experiments (circular dichroism, cell viability, western blot analyses and bipartite-tetracysteine display) confirmed that the set of biotinylated and photo-affinity probes prepared ([B]E1[S], [DB]E1[S] and [BD]E1[S]) were comparable to the previously reported[54] unadorned E1[S] analog in terms of secondary structure, activity, and effect on JM coiled coil formation (Figure S2). The biotinylated and photo-affinity probes containing the sequence of E4[S] ([B]E4[S], [DB]E4[S] and BDE4[S]) also displayed comparable secondary structure and activity to the unadorned E4[S] analog (circular dichroism and cell viability) (Figure S2).

In order to evaluate the photo-induced chemical activity of the diazirine-containing probes, we performed *in vitro* cross-linking and pull-down experiments. Lysates prepared from CHO-K1 cells transiently transfected with either WT EGFR or EGFR-GGS were first incubated for 2h with 25 μM of the biotinylated or photo-affinity probes ([B]E1[S], [DB]E1[S], [BD]E1[S], [B]E4[S], [DB]E4[S] and BDE4[S]), then irradiated with UV light (365 nm) (or not) for

10 min at 4°C. Proteins in the cell lysate that were either non-covalently sequestered or covalently cross-linked were isolated using streptavidin-coated magnetic beads and resolved using SDS-PAGE (Figure 3A). The gels were probed with an anti-EGFR antibody to estimate the relative levels of sequestered WT EGFR or EGFR-GGS and with an anti-biotin antibody to identify cross-linked proteins.

We first analyzed the levels of EGFR sequestered without UV irradiation (Figure 3B). $^{BD}E1^S$ and $^{DB}E1^S$ both sequestered WT EGFR and EGFR-GGS from CHO-K1 cell lysates at levels comparable to $^BE1^S$; in all cases, WT EGFR was sequestered more effectively than EGFR-GGS (which does not contain a native EGFR JM). By contrast, the inactive variants $^BE4^S$, $^{DB}E4^S$ and $^{BD}E4^S$ failed to sequester either WT or EGFR-GGS from cell lysates. Next we analyzed the levels of cross-linked proteins sequestered after UV irradiation (Figure 3C). UV irradiation significantly increased the yield of sequestered WT EGFR, while the yield of sequestered EGFR-GGS increased only modestly (Figure 3C). Lower levels of cross-linked protein were sequestered by the inactive variants $^{DB}E4^S$ and $^{BD}E4^S$ (Figure 3C). Overall, these observations confirm that both $^{DB}E1^S$ and $^{BD}E1^S$ associate with WT EGFR (regardless of the location of the biotin and diazirine moieties), require a native EGFR JM for this association, and possess photo-inducible cross-linking activity. Moreover, the observation that both $^{BD}E1^S$ and $^{DB}E1^S$ (but not $^{DB}E4^S$ and $^{BD}E4^S$) also sequester and cross-link to EGFR-GGS (albeit to a lower extent) emphasizes that interactions outside of the JM segment must also be considered.

EGFR645–1186 is a model for the interaction of E1^S with full length EGFR.

Having validated the activity of photo-affinity probes $^{DB}E1^S$ and $^{BD}E1^S$, we next set out to use them to identify the site(s) of direct interaction with EGFR. For this experiment we made use of soluble EGFR fragments (EGFR645–1186, EGFR672–1186 and EGFR1–621) to simplify identification of the cross-linked site(s) (Figure 4A). Two of the fragments contained the complete EGFR kinase domain (residues 682 – 957) and the C terminal tail (residues 958 – 1186) along with either the complete JM segment (residues 645–681; EGFR645–1186) or a short fragment thereof (residues 672–681; EGFR672–1186). The third EGFR fragment contained only the extracellular domain (residues 1–621, EGFR1–621). We hypothesized that the photo-affinity probes $^{DB}E1^S$ and $^{BD}E1^S$ would associate and cross-link most efficiently to EGFR fragments containing the key interaction surfaces used by E1^S to bind the intact receptor. Based on our previous observations, this EGFR fragment would most likely be the one containing a complete JM segment, namely EGFR645–1186, and not one where the JM is either incomplete (EGFR672–1186) or missing entirely (EGFR1–621).

Solutions of the three EGFR fragments (EGFR645–1186, EGFR672–1186 and EGFR1–621) (0.15 μM) were incubated with increasing concentrations of photo-affinity probes $^{DB}E1^S$ or $^{BD}E1^S$ (0–100 equivalents) for 2 h and then irradiated (365 nm, 10 min). The reaction products were resolved using SDS-PAGE and stained (Silver Stain Plus™) to verify that all samples contained a comparable level of each EGFR fragment (Figure 4A). We next evaluated the yield of cross-linked biotinylated products by immunoblotting with an anti-biotin antibody (Figure 4B). We observed high yields of cross-linked products when $^{DB}E1^S$ and $^{BD}E1^S$ were incubated with EGFR645–1186 (which contains a complete JM segment)

(Figure 4B) but not with either EGFR672–1186 (with a partial JM) or EGFR1–621 (JM is absent), even with a 10-fold excess of the probes (Figure 4B). Overall, our results highlight the need for an intact JM segment for proper interaction of E1^S with the receptor and validate the soluble fragment EGFR645–1186 as a model for this interaction.

Mass spectrometry reveals the locations of cross-links between E1^S photo-affinity probes and EGFR645–1186.

With functional photo-affinity probes (^{DB}E1^S and ^{BD}E1^S) at hand and a suitable system (EGFR645–1186) to model E1^S interactions with EGFR, we proceeded to use high-resolution mass spectrometry (MS) to identify the sites within EGFR645–1186 that become cross-linked to each photo-affinity probe upon irradiation. We incubated EGFR645–1186 (0.15 μM) with 1 equivalent of either ^{DB}E1^S, ^{BD}E1^S, ^{DB}E4^S, or ^{BD}E4^S for 2 h at 4°C, irradiated the solution at 365 nm for 10 min, and digested the reaction mixture with trypsin.[75] The resulting tryptic fragments were subjected to LC-MS/MS analysis using a Q Exactive Orbitrap system and spectra compared with those obtained from a mock reaction that lacked any photoaffinity probe. LC-MS/MS conditions were chosen to ensure adequate coverage of the entire EGFR645–1186 sequence. Comparison of the experimentally obtained MS and MS/MS spectra with the Human Proteome FASTA database using MyriMatch[69] showed that the percent of the EGFR645–1186 sequence found among the tryptic fragments was high: 96.7, 97.9, 93.6, 96.1, and 94.9% for the mock, ^{DB}E1^S, ^{BD}E1^S, ^{DB}E4^S, and ^{BD}E4^S -treated samples, respectively (Table S2, Figure S4).

We next used StavroX [70] to identify peptides whose masses indicated that they were derived from tryptic cleavage of cross-linked EGFR645–1186. StavroX[70] performs in silico proteolysis and effectively acknowledges both the complexity of diazirine insertion reactions and the reality that a cross-linked hydrocarbon-stapled peptide (^{DB}E1^S, ^{BD}E1^S, ^{DB}E4^S or ^{BD}E4^S) can itself undergo tryptic cleavage. The StavroX output consists of a library of virtual MS and MS/MS spectra that can be compared directly with experimental spectra.[70] Each comparison is scored on the basis of the quality of the experimental fragment ion mass spectrum (the number of signals above a specified signal-to-noise ratio) and on the abundance and length of the ionized species. To eliminate false positives, StavroX generates a second virtual library containing the MS and MS/MS spectra expected for reaction and tryptic digestion of the reverse target sequence and calculates a false detection rate (FDR) for each potential match by comparing the scores of the candidate cross-linked peptides obtained from the correct versus the reversed (false-positive) StavroX evaluations. In this work, we retained only the highest scoring cross-linked peptides (FDR < 5%). We then manually inspected the experimental MS/MS spectra of the highest scoring cross-linked peptides to ensure that (1) each represented a cross-link between EGFR645–1186 and the correct diazirine-modified lysine of ^{DB}E1^S, ^{BD}E1^S, ^{DB}E4^S or ^{BD}E4^S; and (2) that the high-resolution b- and y-fragment ions were present and consistent with the candidate cross-linked peptide sequence proposed by StavroX. Of the 107 high-scoring candidate cross-linked peptides identified by StavroX, 27 were manually verified and defined as genuine cross-linked peptides: 24 derived from tryptic cleavage of EGFR645–1186 cross-linked to ^{DB}E1^S, whereas 3 derived from tryptic cleavage of EGFR645–1186 cross-linked to ^{BD}E1^S (Table S3 and S4, Figures S5 and S6). No true-hits were identified in samples of

EGFR645–1186 that had been mock-treated (no probe) or treated with $^{DB}E4^S$ and $^{BD}E4^S$ (negative controls).

Cross-link locations provide evidence for a direct interaction between E1^S and the EGFR JM segment.

The StavroX analysis revealed that E1^S-based photo-affinity probes cross-link to two discrete regions of EGFR645–1186: the JM segment and the C-terminal tail (Figure 5). Of the 27 cross-linked peptides identified as genuine hits, 5 contain sequences from the JM segment and 22 contain sequences from the C-terminal tail. Notably, the patterns of cross-linked products generated by $^{DB}E1^S$ and $^{BD}E1^S$ were not the same: incubation of EGFR645–1186 with $^{DB}E1^S$ led to cross-links within the JM segment (positions 663–664 and 665–666) and the C terminal tail (positions 976–982, 983–991, 1032–1035, 1045–1048, 1137–1139, and 1148–1151, Figure 5A), whereas incubation of EGFR645–1186 with $^{BD}E1^S$ led only to cross-links with the JM segment (positions 663–666 and 669, Figure 5B). These positions are located immediately to the C-terminal side of the JM coiled coil-forming region (positions 650–663, Figure 2A) in a region commonly referred to as JM$_B$. It is worth noting that we did not observe any genuine hits corresponding to cross-links with the N-terminal region of the JM segment (JM$_A$). The JM$_A$ segment of EGFR contains a preponderance of proximal Lys and Arg residues (positions 650–657: VRKRTLRR) (Figure 2A) that obscures the identification of cross-links in this region using mass spectrometry. Nevertheless, the patterns of cross-links induced by $^{DB}E1^S$ and $^{BD}E1^S$ are consistent with a model in which these molecules interact directly with the EGFR JM segment, although we cannot rule out an additional interaction with the C-terminal tail.

What about the C-terminal tail?

The fact that the majority of cross-links observed upon treatment of EGFR645–1186 with $^{DB}E1^S$ fall within the C-terminal tail suggests that either E1^S also interacts directly with the C-terminal tail or that the C-terminal tail (or portions thereof) is proximal to the JM segment. Although the C-terminal tail spans 229 residues (residues 958–1186), only the kinase-proximal region (residues 958–990) has been resolved by crystallography. The high-resolution structure of inactive (symmetric) EGFR dimers containing this kinase-proximal region show C-terminal tail residues 982–990 nestled against the kinase C-lobe surface of the same polypeptide chain in a position that precludes formation of the active, asymmetric kinase dimer.[60,76] The high-resolution structure of the active (asymmetric) EGFR dimer shows the same C-lobe surface on the activator kinase engaged by the C-terminal region of the JM segment (residues 664–670, often referred to as the JM latch[60]), and the C-terminal tail (residues 958–998, albeit with discontinuous electron density) of the receiver kinase engaged with the N- and C-lobes of the activator kinase, within 20 Å of the receiver JM segment.[59]

Evidence that E1^S does not interact directly with the EGFR C-terminal tail.

To determine whether $^{DB}E1^S$ interacts directly with the C-terminal tail, we performed a final set of experiments using expressed EGFR fragments in which portions of the C-terminal tail had been deleted.[76] One variant, EGFR 958–1029, lacked 72 residues found in the N-terminal region of the C-terminal tail (residues 958–1029), while another, EGFR1–998,

lacked 188 residues from the C-terminal region (residues 999–1186). Both of the deleted segments of the C-terminal tail contain residues that were cross-linked to $^{DB}E1^S$ (Figure 6A). To evaluate these interactions, we used CHO-K1 cells transiently transfected to express FLAG-tagged versions of WT EGFR, EGFR1–998, or EGFR 958–1029. Lysates prepared from these cells were incubated for 2 h with 25 μM $^{DB}E1^S$ and irradiated with UV light (365 nm) for 10 min on ice. Proteins sequestered by $^{DB}E1^S$ were isolated by using streptavidin-coated magnetic beads and resolved using SDS PAGE as described previously; the gels were subsequently immuno-blotted to identify the relative levels of each FLAG-tagged EGFR variant (Figure 6C). WT EGFR and EGFR1–998 were expressed in CHO-K1 cells to roughly equivalent levels, while the level of expressed EGFR 958–1029 was reproducibly 30–40% lower (Figure 6B). We reasoned that if $^{DB}E1^S$ binding relied upon a direct interaction with the C-terminal tail, then one or both of the truncated EGFR fragments (EGFR 958–1029 or EGFR1–998) would interact with $^{DB}E1^S$ less favorably than did WT EGFR. This decrease was not observed. The level of EGFR 958–1029 sequestered by $^{DB}E1^S$ was comparable (once normalized for expression) to the level of WT EGFR sequestered, indicating that the presence of residues 958–1029 within the EGFR C-terminal tail are not required for a strong interaction with E1^S. Furthermore, we observed that the level of EGFR1–998 sequestered by $^{DB}E1^S$ was significantly higher (4-fold higher when normalized for expression) than the level of sequestered WT EGFR (Figure 6D). This result implies that E1^S interacts more favorably with EGFR when much (188 residues) of the C-terminal tail is absent, as in EGFR1–998. These observations indicate that (1) the EGFR C-terminal tail does not interact directly with E1^S; and (2) that C-terminal tail residues 999–1186 hinder the interaction between E1^S and EGFR.

DISCUSSION

We previously reported a hydrocarbon-stapled peptide E1^S which, at low micromolar concentrations, decreases the viability of EGFR-expressing cells, down-regulates EGFR autophosphorylation and downstream activators (Erk and Akt), effectively sequesters full length EGFR from CHO-K1 cell lysates, and decreases the extent of coiled coil formation within the JM segment of EGFR dimers assembled on the cell surface.[54] Although these studies pointed circumstantially to a direct interaction between E1^S and the EGFR JM segment, no direct evidence of that interaction was reported.

In this work, we made use of biochemical and cross-linking MS tools to provide direct evidence that E1^S interacts directly with the EGFR JM segment. Traditional pull-down experiments demonstrated that the strongest interaction between E1^S and EGFR in CHO-K1 cell lysates requires an intact, native sequence JM segment. Cross-linking MS experiments revealed a close proximity between the C-terminal region of the JM segment and two complementary diazirine-modified E1^S analogs, $^{DB}E1^S$ and $^{BD}E1^S$. Although the cross-linking MS data additionally revealed a close proximity between $^{DB}E1^S$ and the regions of the EGFR C-terminal tail, subsequent experiments with EGFR fragments lacking two different regions of the C-terminal tail ruled out a direct interaction between E1^S and this region of EGFR.

While the data described above are consistent with a simple model in which E1^S simply binds the EGFR JM of either the activator or receiver kinase to inhibit formation of an activated dimer, several observations suggest a more complex interaction. The first is the relationship between the structure and inhibitory activity of E1^S analogs. Although several (> 11) hydrocarbon-stapled versions of the EGFR JM segment were evaluated as potential EGFR inhibitors,[54,55] only E1^S, with an *i,i+7* hydrocarbon staple between EGFR residues 654 and 661, and E2^S, with a *i,i+4* hydrocarbon staple between EGFR residues 657 and 661, effectively inhibited the proliferation of A431 or H2030 cells, which express WT EGFR (Figure S1).[54] E1^S analogs E4^S, T1^S, and T4^S failed to decrease the proliferation of these two cell lines, as did E3^S, T2^S, and T3^S (Figure S1); these analogs differ from one another only by the location of an *i,i+4* or *i,i+3* hydrocarbon staple (and the amino acid substitutions required for its installation) (Figure 1). The inhibition by E1^S analogs of JM coiled coil formation within EGFR expressed on the cell surface is also dependent on staple location, and in an identical manner (Figure S1). These data suggest that the ability of E1^S to inhibit EGFR relies on a large fraction of its molecular surface – far more than what would be required for a simple paired coiled coil interaction.

The second confounding piece of data, reported here, is the observation of significant cross-links between ^{DB}E1^S and EGFR-GGS,[71] a variant of full length EGFR whose JM sequence is replaced by a repetitive tripeptide repeat (GGS) that lacks the essential elements required for JM coiled coil formation (Figure 2). As noted previously, although an intact, native sequence JM segment is required for the strongest interaction with E1^S, the observation of significant interactions between ^{DB}E1^S and EGFR-GGS suggests that either E1^S binds the JM segment regardless of its sequence, or that it also binds another region of EGFR. Combined with the SAR results, this data raises the possibility that E1^S interacts simultaneously with two regions of EGFR – the JM and someplace else. The final evidence for a more complex E1^S binding mode, also reported here, is the observation that an EGFR deletion fragment lacking the distal region of the C-terminal tail (EGFR1–998) is sequestered by ^{DB}E1^S more than 4-times better than WT EGFR itself (Figure 6), suggesting the involvement of this C-terminal tail region in influencing E1^S binding.

Interpretation of this data in the context of a sophisticated molecular dynamics-derived model of the active full length receptor dimer[5] (Figure 7A) helps provide a consistent picture of the complex interactions between E1^S and EGFR. Several elements of this model[5] are especially notable. First, the model shows the helical region of the receiver kinase JM (residues 645–663) interacting in an antiparallel orientation with the activator kinase JM in a manner that resembles the antiparallel coiled coil observed by NMR.[60,77] In this interaction, the leucine-rich face of the receiver kinase JM faces the leucine-rich face of the activator kinase JM. The model also shows the helical region of the receiver kinase JM (residues 645–663) interacting with the surface of the C-lobe of the activator kinase, with the polar face of the receiver JM facing the activator kinase, and the receiver kinase JM latch (residues 664–681[60]) directly interacting with the activator kinase C-lobe. Finally, the model shows an interaction between the C-terminal tail of the activator kinase (residues 958–995) with the C- and N-lobes of the activator kinase, within 5–20 Å of the receiver JM.[5]

Notably, the details of this model are largely consistent with (1) the only high-resolution crystal structure of the asymmetric (active) EGFR kinase dimer that contains the JM domain (EGFR645–998 K721M; PDB ID: 3GOP)[59] and (2) the structure of the antiparallel JM coiled coil (with or without the appended transmembrane segment) as determined by NMR.[60,77] Importantly, the model is also consistent with bipartite tetracysteine display experiments[61,62] that clearly reveal that the EGFR JM segment can interact with a partner using either the leucine rich face or the polar face. The interactions of the receiver kinase JM described above (Figure 7A) led us to consider three models for the interaction of E1^S with EGFR (Figure 7B). All involve the interaction of a single molecule of E1^S with a single EGFR dimer. In one (Model 1), E1^S interacts with the receiver JM to form an antiparallel coiled coil, displacing the activator JM. In the second (Model 2), E1^S interacts with the activator JM to form an antiparallel coiled coil, displacing the receiver JM. In the third (Model 3), E1^S replaces the receiver JM and interacts simultaneously with both the C-lobe of the activator kinase and the activator JM. To evaluate these three models and guide future experimentation, we considered the locations on EGFR that become cross-linked to ^{DB}E1^S (which carries an N-terminal diazirine) and ^{BD}E1^S (which carries a C-terminal diazirine) within the context of the MD-derived model of full-length EGFR [5] (Figure 7A) as well as the SAR for E1^S analogs discussed above.

Model 1 is not consistent with the different patterns of EGFR cross-links generated by ^{DB}E1^S and ^{BD}E1^S. Interaction of ^{DB}E1^S with the receiver kinase JM in an antiparallel orientation would lead to cross-links with the JM$_B$ region of the receiver kinase but not the C-terminal tail of the activator kinase. Interaction of ^{BD}E1^S with the receiver kinase JM in an antiparallel orientation would lead to cross-links with the C-terminal tail of the activator kinase and the JM$_B$ region of the activator kinase. In this arrangement, one would expect to observe C-terminal tail cross-links using ^{BD}E1^S, which is not what is observed: ^{DB}E1^S generates cross-links to the C-terminal tail (Figure 5A). Model 1 is also not consistent with the E1^S SAR, as it is not obvious why a large fraction of the E1^S molecular surface would be required for this interaction.

Models 2 and 3 are both consistent with the observed patterns of EGFR cross-links. In the case of Model 2, interaction of ^{DB}E1^S with the activator kinase JM in an antiparallel orientation could lead to cross-links with the JM$_B$ region of the activator kinase and its associated C-terminal tail. Interaction of ^{BD}E1^S with the activator kinase JM in an antiparallel orientation would lead to cross-links with only the JM$_B$ region of the receiver kinase. In this arrangement, one would expect to observe both C-terminal tail and JM$_B$ cross-links using ^{DB}E1^S and only JM$_B$ cross-links using ^{BD}E1^S, precisely what is observed (Figure 5A). In the case of Model 3, E1^S replaces the receiver JM to interact simultaneously with both the C-terminal lobe of the activator kinase and the activator kinase JM. This model is expected to generate the same cross-link pattern as Model 2: C-terminal tail and JMB cross-links using ^{DB}E1^S and only JMB cross-links using ^{BD}E1^S, precisely what is observed (Figure 5A). However, Model 3 is more consistent with the previously reported SAR for E1^S analogs: simultaneous interaction of E1^S with the JM and C-lobe of the activator kinase would explain the strict requirement for a large fraction of the E1^S molecular surface.

In summary, here we apply biochemical and cross-linking mass spectrometry tools to increase understanding of how E1[S] interacts with EGFR to allosterically inhibit kinase activity. Our results favor a model (Model 3) in which E1[S] makes use of virtually its entire molecular surface to interact with EGFR. One surface, rich in hydrophobic leucine side chains, interacts in an antiparallel arrangement with the JM segment of the activator kinase. The opposite surface, rich in polar residues, interacts with the C-lobe of the activator kinase to displace the JM latch of the receiver kinase, a region crucial for kinase activation. This model implies that the inhibition of EGFR kinase activity by E1[S] arises not simply from just inhibiting coiled coil formation but in addition by blocking and displacing an intramolecular interaction between the JM latch and the kinase lobe that is essential for formation of the fully active, asymmetric kinase dimer. This complex binding mode provides a structurally well-defined starting point for the design or discovery of more effective peptide mimetics and small molecules that can inhibit EGFR in an analogous way.

Supplementary Material

Refer to Web version on PubMed Central for supplementary material.

ACKNOWLEDGEMENTS

ABBREVIATIONS

EGFR	Epidermal Growth Factor Receptor
TKI	Tyrosine Kinase Inhibitor
JM	Juxtamembrane

REFERENCES

(1). Taylor JM; Mitchell WM; Cohen S. Characterization of the Binding Protein for Epidermal Growth Factor. J. Biol. Chem. 1974, 249 (7), 2188–2194. [PubMed: 4206551]

(2). Cohen S; Carpenter G; King L. Epidermal Growth Factor-Receptor-Protein Kinase Interactions. Co-Purification of Receptor and Epidermal Growth Factor-Enhanced Phosphorylation Activity. J. Biol. Chem. 1980, 255 (10), 4834–4842. [PubMed: 6246084]

(3). Kawamoto T; Sato JD; Le A; Polikoff J; Sato GH; Mendelsohn J. Growth Stimulation of A431 Cells by Epidermal Growth Factor: Identification of High-Affinity Receptors for Epidermal Growth Factor by an Anti-Receptor Monoclonal Antibody. Proc. Natl. Acad. Sci. 1983, 80 (5), 1337–1341. 10.1073/pnas.80.5.1337. [PubMed: 6298788]

(4). Lemmon MA; Schlessinger J. Cell Signaling by Receptor Tyrosine Kinases. Cell 2010, 141 (7), 1117–1134. 10.1016/j.cell.2010.06.011. [PubMed: 20602996]

(5). Arkhipov A; Shan Y; Das R; Endres NF; Eastwood MP; Wemmer DE; Kuriyan J; Shaw DE Architecture and Membrane Interactions of the EGF Receptor. Cell 2013, 152 (3), 557–569. 10.1016/j.cell.2012.12.030. [PubMed: 23374350]

(6). Kovacs E; Zorn JA; Huang Y; Barros T; Kuriyan J. A Structural Perspective on the Regulation of the Epidermal Growth Factor Receptor. Annu Rev Biochem 2015, 84, 739–764. 10.1146/annurev-biochem-060614-034402. [PubMed: 25621509]

(7). Yarden Y; Pines G. The ERBB Network: At Last, Cancer Therapy Meets Systems Biology. Nat. Rev. Cancer 2012, 12 (8), 553–563. 10.1038/nrc3309. [PubMed: 22785351]

(8). Sigismund S; Avanzato D; Lanzetti L. Emerging Functions of the EGFR in Cancer. Mol. Oncol. 2018, 12 (1), 3–20. 10.1002/1878-0261.12155. [PubMed: 29124875]

(9). Herbst RS; Heymach JV; Lippman SM Lung Cancer. N. Engl. J. Med. 2008, 359 (13), 1367–1380. 10.1056/NEJMra0802714. [PubMed: 18815398]

(10). Rotow J; Bivona TG Understanding and Targeting Resistance Mechanisms in NSCLC. Nat. Rev. Cancer 2017, 17 (11), 637–658. 10.1038/nrc.2017.84. [PubMed: 29068003]

(11). Reck M; Rabe KF Precision Diagnosis and Treatment for Advanced Non–Small-Cell Lung Cancer. N. Engl. J. Med. 2017, 377 (9), 849–861. 10.1056/NEJMra1703413. [PubMed: 28854088]

(12). Recondo G; Facchinetti F; Olaussen KA; Besse B; Friboulet L. Making the First Move in EGFR -Driven or ALK -Driven NSCLC: First-Generation or next-Generation TKI? Nat. Rev. Clin. Oncol. 2018, 15 (11), 694–708. 10.1038/s41571-018-0081-4. [PubMed: 30108370]

(13). Ciardiello F; Tortora G. EGFR Antagonists in Cancer Treatment. N. Engl. J. Med. 2008, 358 (11), 1160–1174. 10.1056/NEJMra0707704. [PubMed: 18337605]

(14). Goldstein NI; Prewett M; Zuklys K; Rockwell P; Mendelsohn J. Biological Efficacy of a Chimeric Antibody to the Epidermal Growth Factor Receptor in a Human Tumor Xenograft Model. Clin. Cancer Res. 1995, 1 (11), 1311–1318. [PubMed: 9815926]

(15). Li S; Schmitz KR; Jeffrey PD; Wiltzius JJW; Kussie P; Ferguson KM Structural Basis for Inhibition of the Epidermal Growth Factor Receptor by Cetuximab. Cancer Cell 2005, 7 (4), 301–311. 10.1016/j.ccr.2005.03.003. [PubMed: 15837620]

(16). Jonker DJ; O'Callaghan CJ; Karapetis CS; Zalcberg JR; Tu D; Au H-J; Berry SR; Krahn M; Price T; Simes RJ; Tebbutt NC; van Hazel G; Wierzbicki R; Langer C; Moore MJ Cetuximab for the Treatment of Colorectal Cancer. N. Engl. J. Med. 2007, 357 (20), 2040–2048. 10.1056/NEJMoa071834. [PubMed: 18003960]

(17). Yang X-D; Jia X-C; Corvalan JRF; Wang P; Davis CG Development of ABX-EGF, a Fully Human Anti-EGF Receptor Monoclonal Antibody, for Cancer Therapy. Crit. Rev. Oncol. Hematol. 2001, 38 (1), 17–23. 10.1016/S1040-8428(00)00134-7. [PubMed: 11255078]

(18). Yang X-D; Jia X-C; Corvalan JRF; Wang P; Davis CG; Jakobovits A. Eradication of Established Tumors by a Fully Human Monoclonal Antibody to the Epidermal Growth Factor Receptor without Concomitant Hemotherapy. Cancer Res. 1999, 59 (6), 1236–1243. [PubMed: 10096554]

(19). Mateo C; Moreno E; Amour K; Lombardero J; Harris W; érez R. Humanization of a Mouse Monoclonal Antibody That Blocks the Epidermal Growth Factor Receptor: Recovery of Antagonistic Activity. Immunotechnology 1997, 3 (1), 71–81. 10.1016/S1380-2933(97)00065-1. [PubMed: 9154469]

(20). Liu M; Zhang H; Jimenez X; Ludwig D; Witte L; Bohlen P; Hicklin DJ; Zhu Z. Identification and Characterization of a Fully Human Antibody Directed against Epidermal Growth Factor Receptor for Cancer Therapy. Cancer Res. 2004, 64 (7 Supplement), 163–163.

(21). Thatcher N; Hirsch FR; Luft AV; Szczesna A; Ciuleanu TE; Dediu M; Ramlau R; Galiulin RK; Bálint B; Losonczy G; Kazarnowicz A; Park K; Schumann C; Reck M; Depenbrock H; Nanda S; Kruljac-Letunic A; Kurek R; Paz- Ares L; Socinski MA Necitumumab plus Gemcitabine and Cisplatin versus Gemcitabine and Cisplatin Alone as First-Line Therapy in Patients with Stage IV Squamous Non-Small-Cell Lung Cancer (SQUIRE): An Open-Label, Randomised, Controlled Phase 3 Trial. Lancet Oncol. 2015, 16 (7), 763–774. 10.1016/S1470-2045(15)00021-2. [PubMed: 26045340]

(22). Ferguson FM; Gray NS Kinase Inhibitors: The Road Ahead. Nat. Rev. Drug Discov. 2018, 17 (5), 353–377. 10.1038/nrd.2018.21. [PubMed: 29545548]

(23). Eck MJ; Yun C. Structural and Mechanistic Underpinnings of the Differential Drug Sensitivity of EGFR Mutations in Non-Small Cell Lung Cancer. Biochim. Biophys. Acta 2010, 1804 (3), 559–566. 10.1016/j.bbapap.2009.12.010. [PubMed: 20026433]
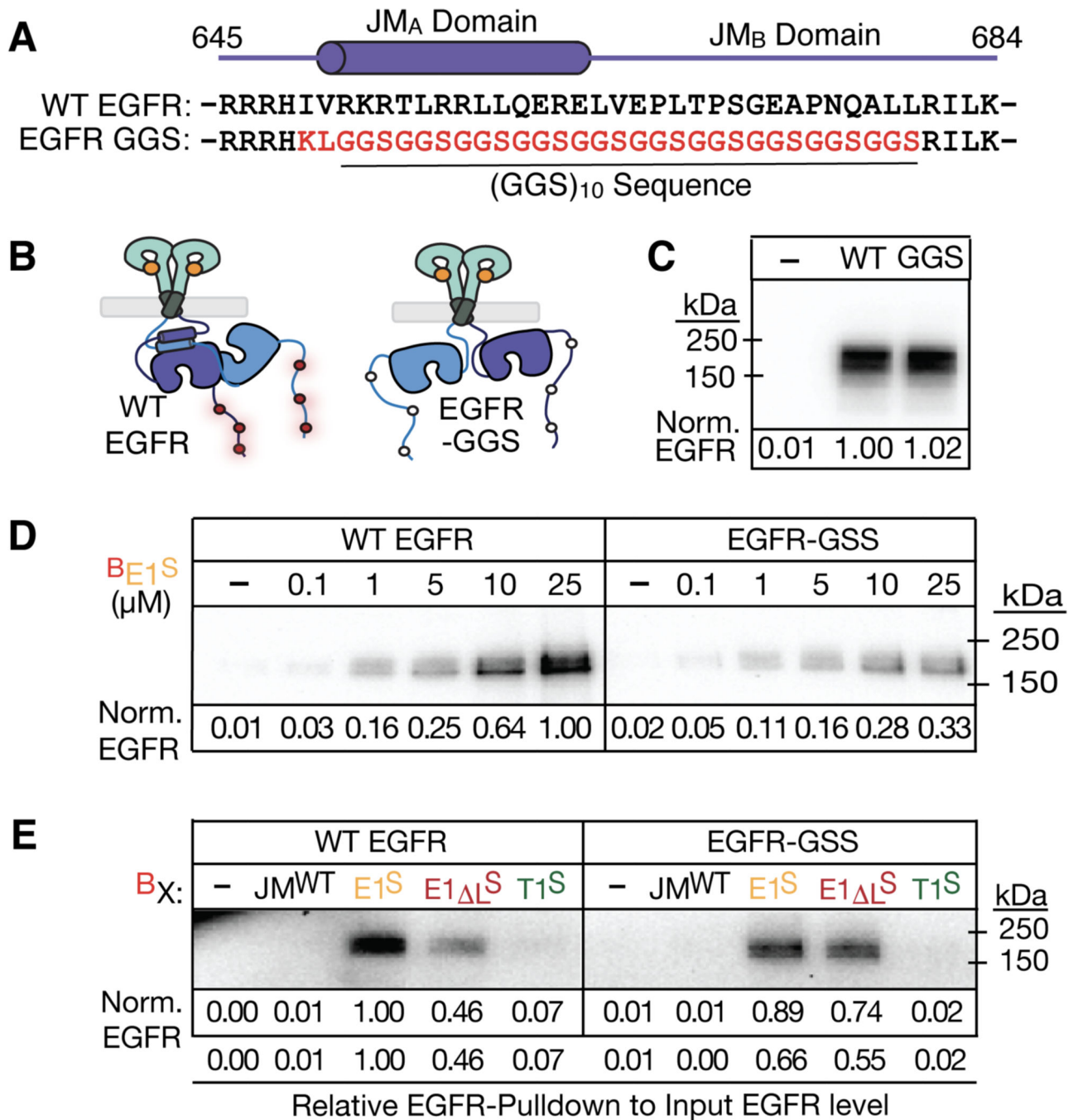
(24). Hidalgo M; Siu LL; Nemunaitis J; Rizzo J; Hammond LA; Takimoto C; Eckhardt SG; Tolcher A; Britten CD; Denis L; Ferrante K; Von Hoff DD; Silberman S; Rowinsky EK Phase I and Pharmacologic Study of OSI-774, an Epidermal Growth Factor Receptor Tyrosine Kinase Inhibitor, in Patients With Advanced Solid Malignancies. J. Clin. Oncol. 2001, 19 (13), 3267–3279. 10.1200/JCO.2001.19.13.3267. [PubMed: 11432895]

(25). Rosell R; Carcereny E; Gervais R; Vergnenegre A; Massuti B; Felip E; Palmero R; Garcia-Gomez R; Pallares C; Sanchez JM; Porta R; Cobo M; Garrido P; Longo F; Moran T; Insa A; De Marinis F; Corre R; Bover I; Illiano A; Dansin E; de Castro J; Milella M; Reguart N; Altavilla G; Jimenez U; Provencio M; Moreno MA; Terrasa J; Muñoz-Langa J; Valdivia J; Isla D; Domine M; Molinier O; Mazieres J; Baize N; Garcia-Campelo R; Robinet G; Rodriguez-Abreu D; Lopez-Vivanco G; Gebbia V; Ferrera-Delgado L; Bombaron P; Bernabe R; Bearz A; Artal A; Cortesi E; Rolfo C; Sanchez-Ronco M; Drozdowskyj A; Queralt C; de Aguirre I; Ramirez JL; Sanchez JJ; Molina MA; Taron M; Paz-Ares L. Erlotinib versus Standard Chemotherapy as First-Line Treatment for European Patients with Advanced EGFR Mutation-Positive Non-Small-Cell Lung Cancer (EURTAC): A Multicentre, Open-Label, Randomised Phase 3 Trial. Lancet Oncol. 2012, 13 (3), 239–246. 10.1016/S1470-2045(11)70393-X. [PubMed: 22285168]

(26). Wakeling AE; Guy SP; Woodburn JR; Ashton SE; Curry BJ; Barker AJ; Gibson KH ZD1839 (Iressa): An Orally Active Inhibitor of Epidermal Growth Factor Signaling with Potential for Cancer Therapy. Cancer Res. 2002, 62 (20), 5749–5754. [PubMed: 12384534]

(27). Maemondo M; Inoue A; Kobayashi K; Sugawara S; Oizumi S; Isobe H; Gemma A; Harada M; Yoshizawa H; Kinoshita I; Fujita Y; Okinaga S; Hirano H; Yoshimori K; Harada T; Ogura T; Ando M; Miyazawa H; Tanaka T; Saijo Y; Hagiwara K; Morita S; Nukiwa T. Gefitinib or Chemotherapy for Non–Small-Cell Lung Cancer with Mutated EGFR. N. Engl. J. Med. 2010, 362 (25), 2380–2388. 10.1056/NEJMoa0909530. [PubMed: 20573926]

(28). Lynch TJ; Okimoto RA; Supko JG; Settleman J. Activating Mutations in the Epidermal Growth Factor Receptor Underlying Responsiveness of Non–Small-Cell Lung Cancer to Gefitinib. N. Engl. J. Med. 2004, 11.

(29). Paez JG; Jänne PA; Lee JC; Tracy S; Greulich H; Gabriel S; Herman P; Kaye FJ; Lindeman N; Boggon TJ; Naoki K; Sasaki H; Fujii Y; Eck MJ; Sellers WR; Johnson BE; Meyerson M. EGFR Mutations in Lung Cancer: Correlation with Clinical Response to Gefitinib Therapy. Science 2004, 304 (5676), 1497–1500. 10.1126/science.1099314. [PubMed: 15118125]

(30). Pao W; Miller V; Zakowski M; Doherty J; Politi K; Sarkaria I; Singh B; Heelan R; Rusch V; Fulton L; Mardis E; Kupfer D; Wilson R; Kris M; Varmus H. EGF Receptor Gene Mutations Are Common in Lung Cancers from "Never Smokers" and Are Associated with Sensitivity of Tumors to Gefitinib and Erlotinib. Proc. Natl. Acad. Sci. 2004, 101 (36), 13306–13311. 10.1073/pnas.0405220101. [PubMed: 15329413]

(31). COSMIC. Catalogue of Somatic Mutations in Cancer, Release Version 92. 2020.

(32). Graham RP; Treece AL; Lindeman NI; Vasalos P; Shan Mu; Jennings LJ; Rimm DL Worldwide Frequency of Commonly Detected EGFR Mutations. Arch. Pathol. Lab. Med. 2017, 142 (2), 163–167. 10.5858/arpa.2016-0579-CP. [PubMed: 29106293]

(33). Sharma SV; Bell DW; Settleman J; Haber DA Epidermal Growth Factor Receptor Mutations in Lung Cancer. Nat. Rev. Cancer 2007, 7 (3), 169–181. 10.1038/nrc2088. [PubMed: 17318210]

(34). Li D; Ambrogio L; Shimamura T; Kubo S; Takahashi M; Chirieac LR; Padera RF; Shapiro GI; Baum A; Himmelsbach F; Rettig WJ; Meyerson M; Solca F; Greulich H; Wong K-K BIBW2992, an Irreversible EGFR/HER2 Inhibitor Highly Effective in Preclinical Lung Cancer Models. Oncogene 2008, 27 (34), 4702–4711. 10.1038/onc.2008.109. [PubMed: 18408761]

(35). Sequist LV; Soria J-C; Goldman JW; Wakelee HA; Gadgeel SM; Varga A; Papadimitrakopoulou V; Solomon BJ; Oxnard GR; Dziadziuszko R; Aisner DL; Doebele RC; Galasso C; Garon EB; Heist RS; Logan J; Neal JW; Mendenhall MA; Nichols S; Piotrowska Z; Wozniak AJ; Raponi M; Karlovich CA; Jaw-Tsai S; Isaacson J; Despain D; Matheny SL; Rolfe L; Allen AR; Camidge DR Rociletinib in EGFR-Mutated Non–Small-Cell Lung Cancer. N. Engl. J. Med. 2015, 372 (18), 1700–1709. 10.1056/NEJMoa1413654. [PubMed: 25923550]

(36). Walter AO; Sjin RTT; Haringsma HJ; Ohashi K; Sun J; Lee K; Dubrovskiy A; Labenski M; Zhu Z; Wang Z; Sheets M; Martin TS; Karp R; Kalken D. van; Chaturvedi P; Niu D; Nacht M; Petter RC; Westlin W; Lin K; Jaw-Tsai S; Raponi M; Dyke TV; Etter J; Weaver Z; Pao W; Singh

J; Simmons AD; Harding TC; Allen A. Discovery of a Mutant-Selective Covalent Inhibitor of EGFR That Overcomes T790M-Mediated Resistance in NSCLC. Cancer Discov. 2013, 3 (12), 1404–1415. 10.1158/2159-8290.CD-13-0314. [PubMed: 24065731]

(37). Zhou W; Ercan D; Chen L; Yun C-H; Li D; Capelletti M; Cortot AB; Chirieac L; Iacob RE; Padera R; Engen JR; Wong K-K; Eck MJ; Gray NS; Jänne PA Novel Mutant-Selective EGFR Kinase Inhibitors against EGFR T790M. Nature 2009, 462 (7276), 1070–1074. 10.1038/nature08622. [PubMed: 20033049]

(38). Cross DAE; Ashton SE; Ghiorghiu S; Eberlein C; Nebhan CA; Spitzler PJ; Orme JP; Finlay MRV; Ward RA; Mellor MJ; Hughes G; Rahi A; Jacobs VN; Brewer MR; Ichihara E; Sun J; Jin H; Ballard P; Al-Kadhimi K; Rowlinson R; Klinowska T; Richmond GHP; Cantarini M; Kim D-W; Ranson MR; Pao W. AZD9291, an Irreversible EGFR TKI, Overcomes T790M-Mediated Resistance to EGFR Inhibitors in Lung Cancer. Cancer Discov. 2014, 4 (9), 1046–1061. 10.1158/2159-8290.CD-14-0337. [PubMed: 24893891]

(39). Soria J-C; Ohe Y; Vansteenkiste J; Reungwetwattana T; Chewaskulyong B; Lee KH; Dechaphunkul A; Imamura F; Nogami N; Kurata T; Okamoto I; Zhou C; Cho BC; Cheng Y; Cho EK; Voon PJ; Planchard D; Su W-C; Gray JE; Lee SM; Hodge R; Marotti M; Rukazenkov Y; Ramalingam SS Osimertinib in Untreated EGFR-Mutated Advanced Non–Small-Cell Lung Cancer. N. Engl. J. Med. 2017. 10.1056/NEJMoa1713137.

(40). Ramalingam SS; Vansteenkiste J; Planchard D; Cho BC; Gray JE; Ohe Y; Zhou C; Reungwetwattana T; Cheng Y; Chewaskulyong B; Shah R; Cobo M; Lee KH; Cheema P; Tiseo M; John T; Lin M-C; Imamura F; Kurata T; Todd A; Hodge R; Saggese M; Rukazenkov Y; Soria J-C Overall Survival with Osimertinib in Untreated, EGFR-Mutated Advanced NSCLC. N. Engl. J. Med. 2020, 382 (1), 41–50. 10.1056/NEJMoa1913662. [PubMed: 31751012]

(41). Burslem GM; Smith BE; Lai AC; Jaime-Figueroa S; McQuaid DC; Bondeson DP; Toure M; Dong H; Qian Y; Wang J; Crew AP; Hines J; Crews CM The Advantages of Targeted Protein Degradation over Inhibition: A RTK Case Study. Cell Chem. Biol. 2018, 25 (1), 67–77.e3. 10.1016/j.chembiol.2017.09.009. [PubMed: 29129716]

(42). Iradyan M; Iradyan N; Hulin P; Hambardzumyan A; Gyulkhandanyan A; Alves de Sousa R; Hessani A; Roussakis C; Bollot G; Bauvais C; Sakanyan V. Targeting Degradation of EGFR through the Allosteric Site Leads to Cancer Cell Detachment-Promoted Death. Cancers 2019, 11 (8), 1094. 10.3390/cancers11081094.

(43). Cheng M; Yu X; Lu K; Xie L; Wang L; Meng F; Han X; Chen X; Liu J; Xiong Y; Jin J. Discovery of Potent and Selective Epidermal Growth Factor Receptor (EGFR) Bifunctional Small-Molecule Degraders. J. Med. Chem. 2020, 63 (3), 1216–1232. 10.1021/acs.jmedchem.9b01566. [PubMed: 31895569]

(44). Jang J; To C; Clercq DJHD; Park E; Ponthier CM; Shin BH; Mushajiang M; Nowak RP; Fischer ES; Eck MJ; Jänne PA; Gray NS Mutant-Selective Allosteric EGFR Degraders Are Effective Against a Broad Range of Drug-Resistant Mutations. Angew. Chem. 2020, 132 (34), 14589–14597. 10.1002/ange.202003500.

(45). Zhang H; Zhao H-Y; Xi X-X; Liu Y-J; Xin M; Mao S; Zhang J-J; Lu A-X; Zhang S-Q Discovery of Potent Epidermal Growth Factor Receptor (EGFR) Degraders by Proteolysis Targeting Chimera (PROTAC). Eur. J. Med. Chem. 2020, 189, 112061. 10.1016/j.ejmech.2020.112061.

(46). Zhao H-Y; Yang X-Y; Lei H; Xi X-X; Lu S-M; Zhang J-J; Xin M; Zhang S-Q Discovery of Potent Small Molecule PROTACs Targeting Mutant EGFR. Eur. J. Med. Chem. 2020, 208, 112781. 10.1016/j.ejmech.2020.112781.

(47). He K; Zhang Z; Wang W; Zheng X; Wang X; Zhang X. Discovery and Biological Evaluation of Proteolysis Targeting Chimeras (PROTACs) as an EGFR Degraders Based on Osimertinib and Lenalidomide. Bioorg. Med. Chem. Lett. 2020, 30 (12), 127167. 10.1016/j.bmcl.2020.127167.

(48). Banik SM; Pedram K; Wisnovsky S; Ahn G; Riley NM; Bertozzi CR Lysosome-Targeting Chimaeras for Degradation of Extracellular Proteins. Nature 2020, 584 (7820), 291–297. 10.1038/s41586-020-2545-9. [PubMed: 32728216]

(49). Jia Y; Yun C-H; Park E; Ercan D; Manuia M; Juarez J; Xu C; Rhee K; Chen T; Zhang H; Palakurthi S; Jang J; Lelais G; DiDonato M; Bursulaya B; Michellys P-Y; Epple R; Marsilje TH; McNeill M; Lu W; Harris J; Bender S; Wong KK; Jänne PA; Eck MJ Overcoming

EGFR(T790M) and EGFR(C797S) Resistance with Mutant-Selective Allosteric Inhibitors. Nature 2016, 534 (7605), 129–132. 10.1038/nature17960. [PubMed: 27251290]

(50). To C; Jang J; Chen T; Park E; Mushajiang M; De Clercq DJH; Xu M; Wang S; Cameron MD; Heppner DE; Shin BH; Gero TW; Yang A; Dahlberg SE; Wong K-K; Eck MJ; Gray NS; Jänne PA Single and Dual Targeting of Mutant EGFR with an Allosteric Inhibitor. Cancer Discov. 2019, 9 (7), 926–943. 10.1158/2159-8290.CD-18-0903. [PubMed: 31092401]

(51). Thress KS; Paweletz CP; Felip E; Cho BC; Stetson D; Dougherty B; Lai Z; Markovets A; Vivancos A; Kuang Y; Ercan D; Matthews SE; Cantarini M; Barrett JC; Jänne PA; Oxnard GR Acquired EGFR C797S Mutation Mediates Resistance to AZD9291 in Non–Small Cell Lung Cancer Harboring EGFR T790M. Nat. Med. 2015, 21 (6), 560–562. 10.1038/nm.3854. [PubMed: 25939061]

(52). Boran ADW; Seco J; Jayaraman V; Jayaraman G; Zhao S; Reddy S; Chen Y; Iyengar R. A Potential Peptide Therapeutic Derived from the Juxtamembrane Domain of the Epidermal Growth Factor Receptor. PLOS ONE 2012, 7 (11), e49702. 10.1371/journal.pone.0049702.

(53). Hart MR; Su H-Y; Broka D; Goverdhan A; Schroeder JA Inactive ERBB Receptors Cooperate With Reactive Oxygen Species To Suppress Cancer Progression. Mol. Ther. 2013, 21 (11), 1996– 2007. 10.1038/mt.2013.196. [PubMed: 24081029]

(54). Sinclair JK-L; Denton EV; Schepartz A. Inhibiting Epidermal Growth Factor Receptor at a Distance. J. Am. Chem. Soc. 2014, 136 (32), 11232–11235. 10.1021/ja504076t. [PubMed: 25075632]

(55). Sinclair JK-L; Schepartz A. Influence of Macrocyclization on Allosteric, Juxtamembrane-Derived, Stapled Peptide Inhibitors of the Epidermal Growth Factor Receptor (EGFR). Org. Lett. 2014, 16 (18), 4916–4919. 10.1021/ol502426b. [PubMed: 25207804]

(56). Gerhart J; Thévenin AF; Bloch E; King KE; Thévenin D. Inhibiting Epidermal Growth Factor Receptor Dimerization and Signaling Through Targeted Delivery of a Juxtamembrane Domain Peptide Mimic. ACS Chem. Biol. 2018, 13 (9), 2623–2632. 10.1021/acschembio.8b00555. [PubMed: 30133245]

(57). Eissa NG; Sayers EJ; Birch D; Patel SG; Tsai Y-H; Nielsen HM; Jones AT EJP18 Peptide Derived from the Juxtamembrane Domain of Epidermal Growth Factor Receptor Represents a Novel Membrane-Active Cell-Penetrating Peptide. Biochem. J. 2020, 477 (1), 45–60. 10.1042/BCJ20190452. [PubMed: 31820794]

(58). Liu Q; Zhou J; Gao J; Ma W; Wang S; Xing L. Rational Design of EGFR Dimerization-Disrupting Peptides: A New Strategy to Combat Drug Resistance in Targeted Lung Cancer Therapy. Biochimie 2020, 176, 128–137. 10.1016/j.biochi.2020.07.010. [PubMed: 32721503]

(59). Brewer MR; Choi SH; Alvarado D; Moravcevic K; Pozzi A; Lemmon MA; Carpenter G. The Juxtamembrane Region of the EGF Receptor Functions as an Activation Domain. Mol. Cell 2009, 34 (6), 641–651. 10.1016/j.molcel.2009.04.034. [PubMed: 19560417]

(60). Jura N; Endres NF; Engel K; Deindl S; Das R; Lamers MH; Wemmer DE; Zhang X; Kuriyan J. Mechanism for Activation of the EGF Receptor Catalytic Domain by the Juxtamembrane Segment. Cell 2009, 137 (7), 1293–1307. 10.1016/j.cell.2009.04.025. [PubMed: 19563760]

(61). Scheck RA; Lowder MA; Appelbaum JS; Schepartz A. Bipartite Tetracysteine Display Reveals Allosteric Control of Ligand-Specific EGFR Activation. ACS Chem Biol 2012, 7 (8), 1367– 1376. 10.1021/cb300216f. [PubMed: 22667988]

(62). Doerner A; Scheck R; Schepartz A. Growth Factor Identity Is Encoded by Discrete Coiled-Coil Rotamers in the EGFR Juxtamembrane Region. Chem Biol 2015, 22 (6), 776–784. 10.1016/j.chembiol.2015.05.008. [PubMed: 26091170]

(63). Sinclair JKL; Walker AS; Doerner AE; Schepartz A. Mechanism of Allosteric Coupling into and through the Plasma Membrane by EGFR. Cell Chem Biol 2018, 25 (7), 857–870 e7. 10.1016/j.chembiol.2018.04.005. [PubMed: 29731426]

(64). Schafmeister CE; Po J; Verdine GL An All-Hydrocarbon Cross-Linking System for Enhancing the Helicity and Metabolic Stability of Peptides. J. Am. Chem. Soc. 2000, 122 (24), 5891–5892. 10.1021/ja000563a.

(65). Verdine GL; Hilinski GJ All-Hydrocarbon Stapled Peptides as Synthetic Cell-Accessible Mini-Proteins. Drug Discov. Today Technol. 2012, 9 (1), e41–e47. 10.1016/j.ddtec.2012.01.004.

(66). Walensky LD; Bird GH Hydrocarbon-Stapled Peptides: Principles, Practice, and Progress. J. Med. Chem. 2014, 57 (15), 6275–6288. 10.1021/jm4011675. [PubMed: 24601557]

(67). Pao W; Miller VA; Politi KA; Riely GJ; Somwar R; Zakowski MF; Kris MG; Varmus H. Acquired Resistance of Lung Adenocarcinomas to Gefitinib or Erlotinib Is Associated with a Second Mutation in the EGFR Kinase Domain. PLOS Med. 2005, 2 (3), e73. 10.1371/journal.pmed.0020073. [PubMed: 15737014]

(68). Scheck RA; Schepartz A. Surveying Protein Structure and Function Using Bis-Arsenical Small Molecules. Acc Chem Res 2011, 44 (9), 654–665. 10.1021/ar2001028. [PubMed: 21766813]

(69). Tabb DL; Fernando CG; Chambers MC MyriMatch: Highly Accurate Tandem Mass Spectral Peptide Identification by Multivariate Hypergeometric Analysis. J. Proteome Res. 2007, 6 (2), 654–661. 10.1021/pr0604054. [PubMed: 17269722]

(70). Götze M; Pettelkau J; Schaks S; Bosse K; Ihling CH; Krauth F; Fritzsche R; Kühn U; Sinz A. StavroX—A Software for Analyzing Crosslinked Products in Protein Interaction Studies. J. Am. Soc. Mass Spectrom. 2012, 23 (1), 76–87. 10.1021/jasms.8b04122. [PubMed: 22038510]

(71). He L; Hristova K. Consequences of Replacing EGFR Juxtamembrane Domain with an Unstructured Sequence. Sci. Rep. 2012, 2 (1), 854. 10.1038/srep00854. [PubMed: 23152945]

(72). MacKinnon AL; Taunton J. Target Identification by Diazirine Photo-Cross-Linking and Click Chemistry. Curr. Protoc. Chem. Biol. 2009, 1 (1), 55–73. 10.1002/9780470559277.ch090167. [PubMed: 23667793]

(73). Park J; Koh M; Koo JY; Lee S; Park SB Investigation of Specific Binding Proteins to Photoaffinity Linkers for Efficient Deconvolution of Target Protein. ACS Chem. Biol. 2016, 11 (1), 44–52. 10.1021/acschembio.5b00671. [PubMed: 26502221]

(74). Tanaka Y; Bond MR; Kohler JJ Photocrosslinkers Illuminate Interactions in Living Cells. Mol. Biosyst. 2008, 4 (6), 473–480. 10.1039/B803218A. [PubMed: 18493640]

(75). Saveliev S; Bratz M; Zubarev R; Szapacs M; Budamgunta H; Urh M. Trypsin/LysC Protease Mix for Enhanced Protein Mass Spectrometry Analysis. Nat. Methods 2013, 10 (11), i–ii. 10.1038/nmeth.f.371.

(76). Kovacs E; Das R; Wang Q; Collier TS; Cantor A; Huang Y; Wong K; Mirza A; Barros T; Grob P; Jura N; Bose R; Kuriyan J. Analysis of the Role of the C-Terminal Tail in the Regulation of the Epidermal Growth Factor Receptor. Mol. Cell. Biol. 2015, 35 (17), 3083–3102. 10.1128/MCB.00248-15. [PubMed: 26124280]

(77). Endres NF; Das R; Smith AW; Arkhipov A; Kovacs E; Huang Y; Pelton JG; Shan Y; Shaw DE; Wemmer DE; Groves JT; Kuriyan J. Conformational Coupling across the Plasma Membrane in Activation of the EGF Receptor. Cell 2013, 152 (3), 543–556. 10.1016/j.cell.2012.12.032. [PubMed: 23374349]

Figure 1.
Design of stapled peptides targeting specific JM interfaces (A) Sequences of the EGFR juxtamembrane (JM) segment (EGFR residues 645–671) and hydrocarbon-stapled peptides studied herein. Shown are the locations of unnatural amino acids (R)-2-(7′-octenyl)alanine (Z), (S)-2-(4′-pentenyl)-alanine (X), and (R)-2-(4′-pentenyl)-alanine (B) used to install *i,i+3, i,i+4,* or *i,i+7* cross-links between the indicated residues. (B) Helical wheel representation of the hydrocarbon-stapled peptides shown in (A). The leucine-rich and polar faces of the peptides are highlighted in red and blue, respectively. **See also** Figure S1.

Figure 2.
A wild type JM sequence is necessary for the interaction of EGFR with E1^S. (A) JM
sequences of WT EGFR and EGFR-GGS (residues 645–684). WT EGFR residues mutated
in EGFR-GGS are highlighted in red. (B) Cartoon illustrating the domains of WT EGFR and
EGFR-GGS. EGFR-GGS lacking the native JM is unable to activate the kinase (C) Relative
levels of expressed EGFR in lysates prepared from CHO-K1 cells transfected with plasmids
encoding WT EGFR (WT) or EGFR-GGS (GGS). (D and E) Immunoblots illustrating the
relative levels of WT EGFR or EGFR-GSS sequestered from lysates of CHO-K1 cells

expressing these variants, incubated with (D) the indicated concentration (μM) of ^{B}E1^S or (E) 25 μuM of biotinylated analogs ^{B}JM^{WT}, ^{B}E1^S, ^{B}E1 $_L$^{S} and ^{B}T1^S. The fraction of EGFR sequestered was normalized to the fraction of WT EGFR sequestered by 25 μM ^{B}E1^S. Band intensities were quantified with ImageJ (v.1.46r). The values shown represent the average of 3 independent replicates.
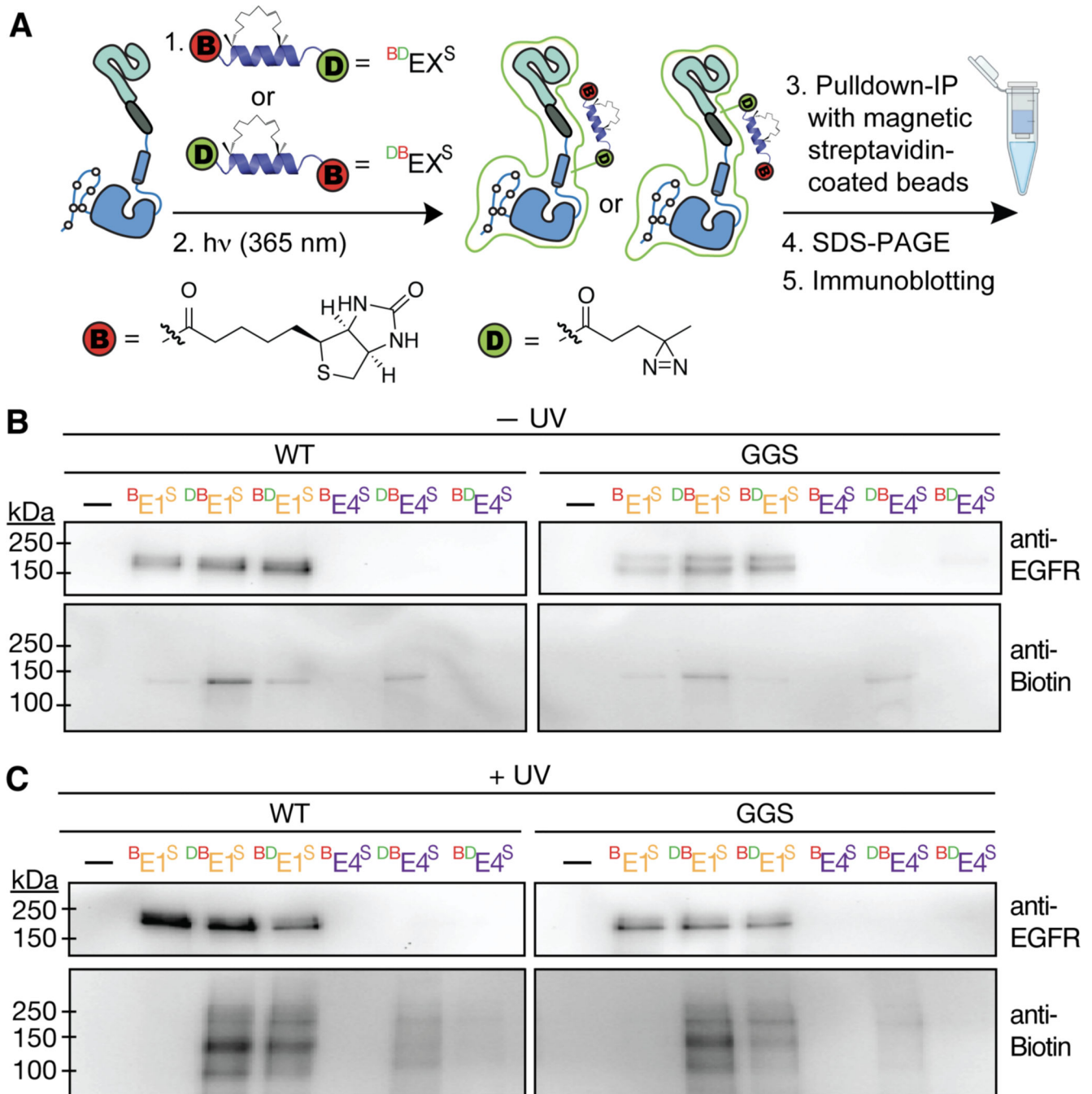
Figure 3.
Photo-affinity labeling experiments confirm that an intact, native sequence juxtamembrane segment is required for a high affinity interaction between E1^S and EGFR. (A) Scheme illustrating potential cross-linking reactions between EGFR and either ^{BD}E1^S, ^{DB}E1^S, BDE4^S or ^{DB}E4^S. (B,C) Immunoblots illustrating proteins sequestered by biotinylated photo-affinity probes without (B) or with (C) irradiation at 365 nm. Lysates of 10^6 transiently transfected CHO-K1 cells were treated for 2 h with 25 μM of the indicated molecule (^{BD}E1^S, DBE1^S, ^{B}E1^S, ^{BD}E4^S, ^{DB}E4^S, or ^{B}E4^S) and irradiated (or not) for 10

min at 4°C. Treated lysates (in 300 μL of Binding Buffer) were then incubated overnight with 100 μL streptavidin coated-beads (Streptavidin Mag Sepharose beads), washed, and the proteins eluted using 2% SDS buffer. Sequestered proteins were resolved using SDS-PAGE (10% polyacrylamide) and immuno-blotted to detect EGFR or biotin. The relative WT:GGS-EGFR levels in lysates were 1:1.5. See also Figures S2 and S3
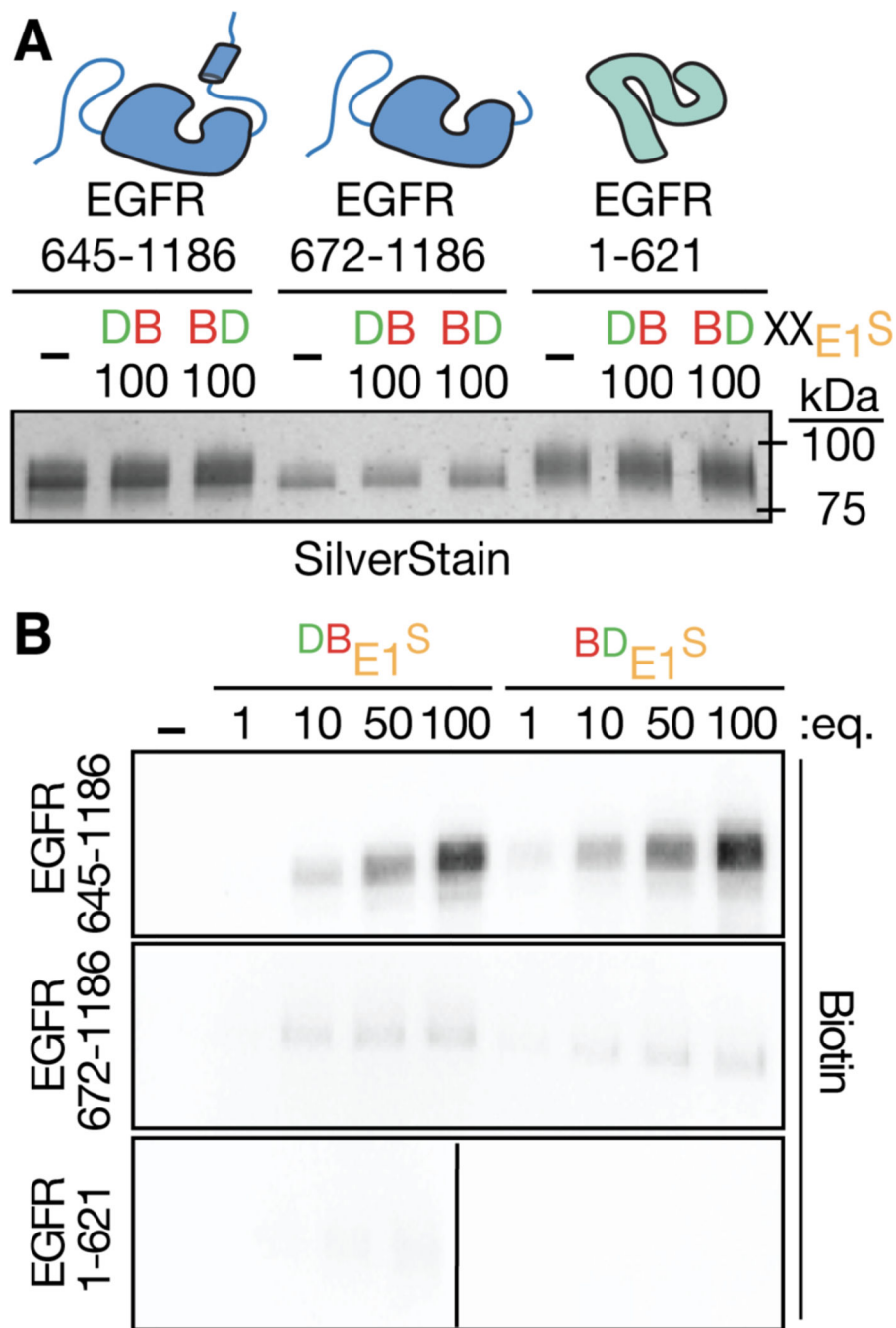
Figure 4.
EGFR645–1186 is a model for the interaction of E1[S] with full length EGFR in cells. (A) Silver Stain blots illustrating the relative concentration of EGFR fragments EGFR645–1186, EGFR672–1186, or EGFR1–621 (0.15 μM) incubated with 0 or 100 equivalents [DB]E1[S] or [BD]E1[S] for 2 h, then irradiated (365 nm,10 min). Samples were resolved by SDS-PAGE (10% polyacrylamide) and stained with Silver Stain PlusTM (BioRad) (B) Immunoblots illustrating the relative amounts of biotinylated fragments EGFR645–1186, EGFR672–1186, or EGFR1–621 post- incubation with 0, 1, 10, 50 or 100 equivalents of [DB]E1[S] or [BD]E1[S] for

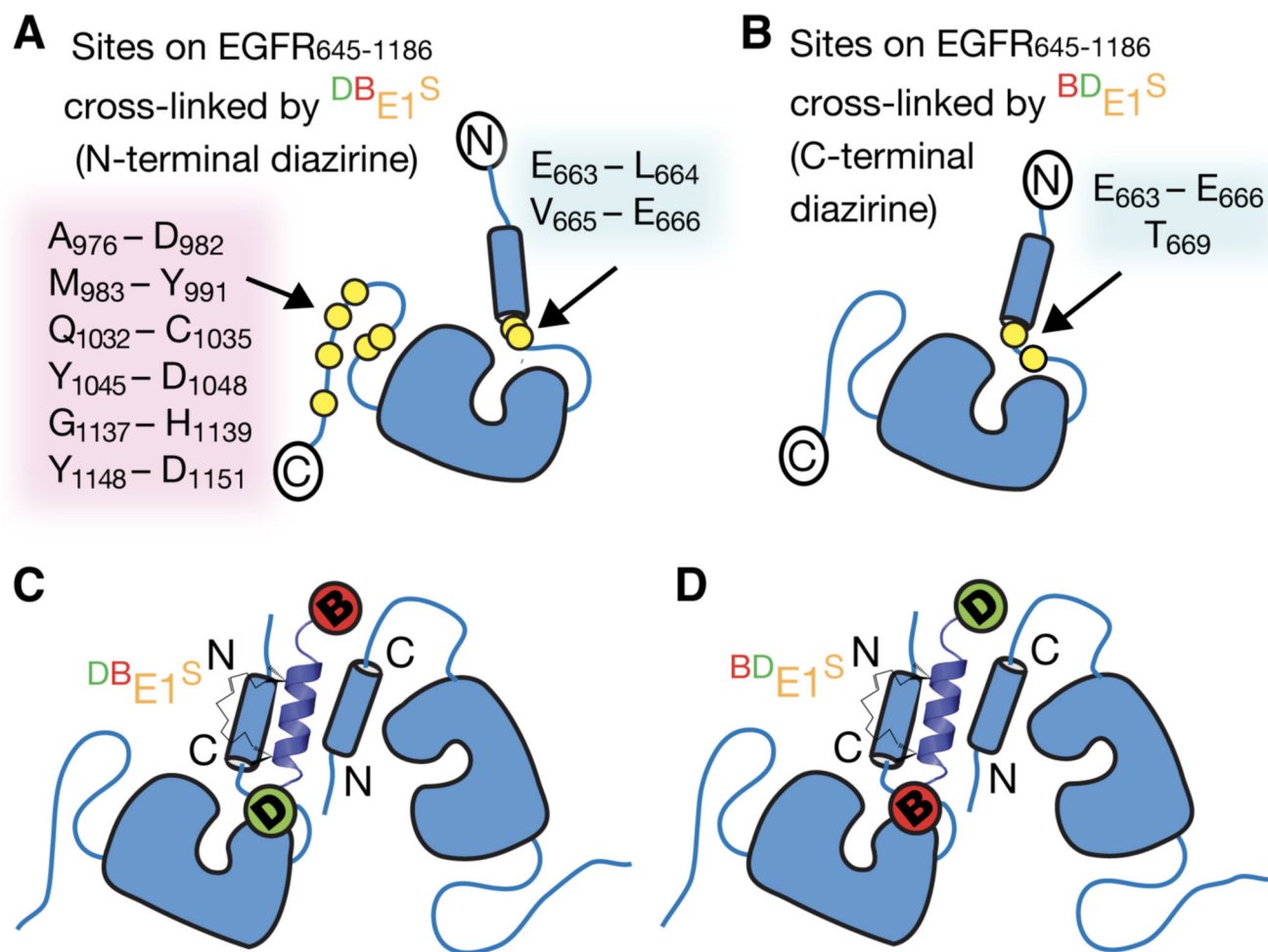2 h, irradiated, resolved and immunoblotted using an anti-Biotin antibody. See also Figure S3.

Figure 5.
Mass spectrometry reveals the locations of cross-links between E1^S photo-affinity probes and EGFR645–1186. Cartoon representation of the sites within EGFR645–1186 that become cross-linked (indicated by yellow dots) to (A) ^{DB}E1^S or (B) ^{BD}E1^S. Models representing potential modes of binding of (C) ^{DB}E1^S or (D) ^{BD}E1^S to the JM segment of EGFR645–1186, in an antiparallel orientation. See also Figures S4, S5 and S6.
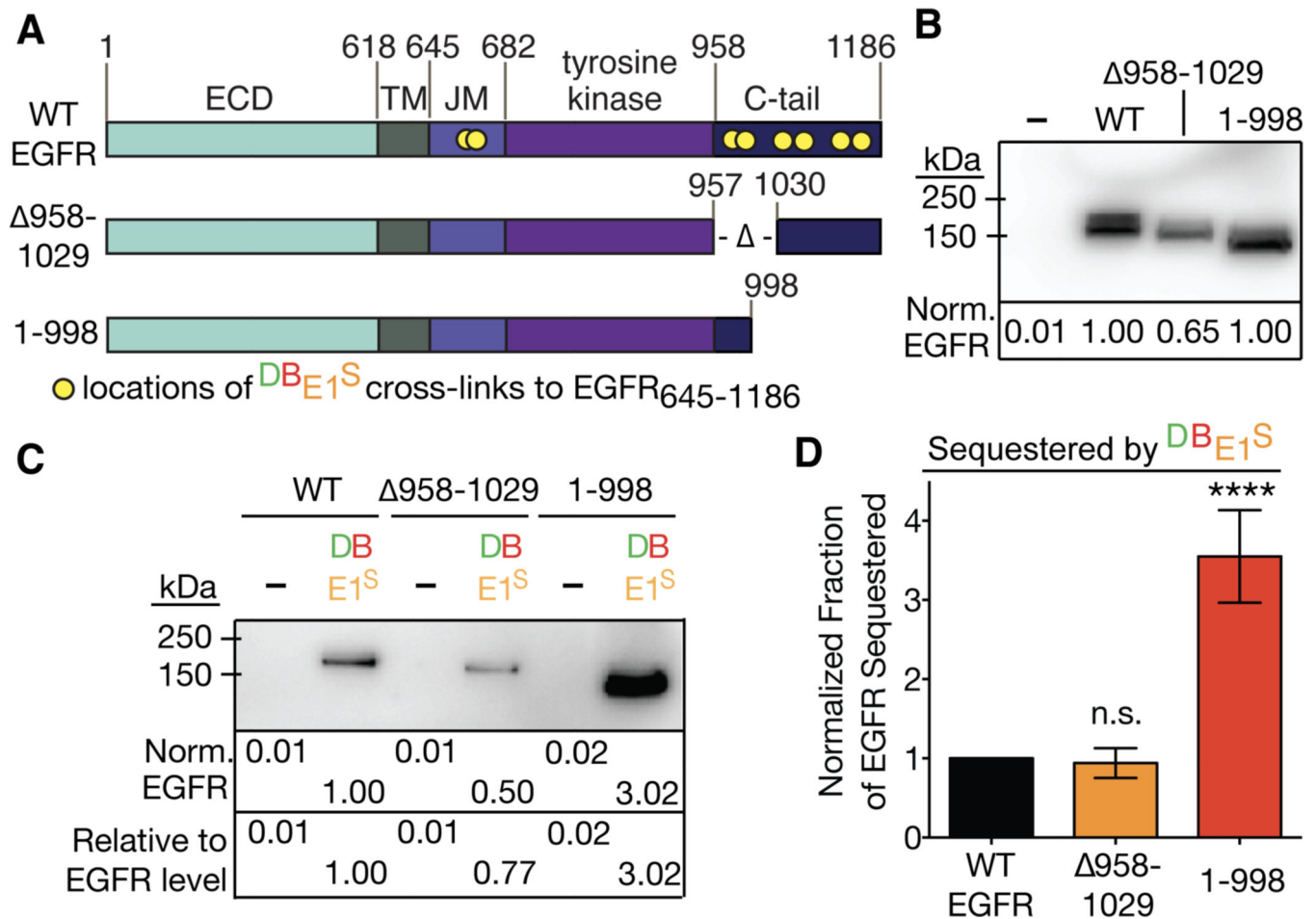
Figure 6.
Evidence that E1^S does not interact directly with the EGFR C-terminal tail. (A) Domain architecture of WT EGFR and EGFR fragments EGFR 958–1029 or EGFR1–998 used in this study. The locations of the cross-links between ^{DB}E1^S and EGFR645–1186 are indicated by yellow dots. (B) Relative levels of FLAG-tagged proteins detected in lysates prepared from CHO-K1 cells transiently transfected with plasmids encoding FLAG-tagged WT EGFR, EGFR 958–1029, or EGFR1–998. Lysates were prepared and analyzed as described in the legend for Figure 3, but immunoblotted with an anti-FLAG antibody. (C) Western blot illustrating the relative levels of the indicated FLAG-tagged proteins sequestered after treatment with ^{DB}E1^S, irradiation, and overnight incubation with streptavidin coated-beads. (D) The intensities of FLAG-tagged bands in six replicate assays were measured, normalized to the level of WT EGFR sequestered by 25 μM of ^{DB}E1^S, and plotted. Error bars represent the standard error of the mean: ****$p < 0.0001$; one-way ANOVA with Dunnett post-analysis accounting for multiple comparisons. Protein band intensities were measured using ImageJ, version 1.46r.
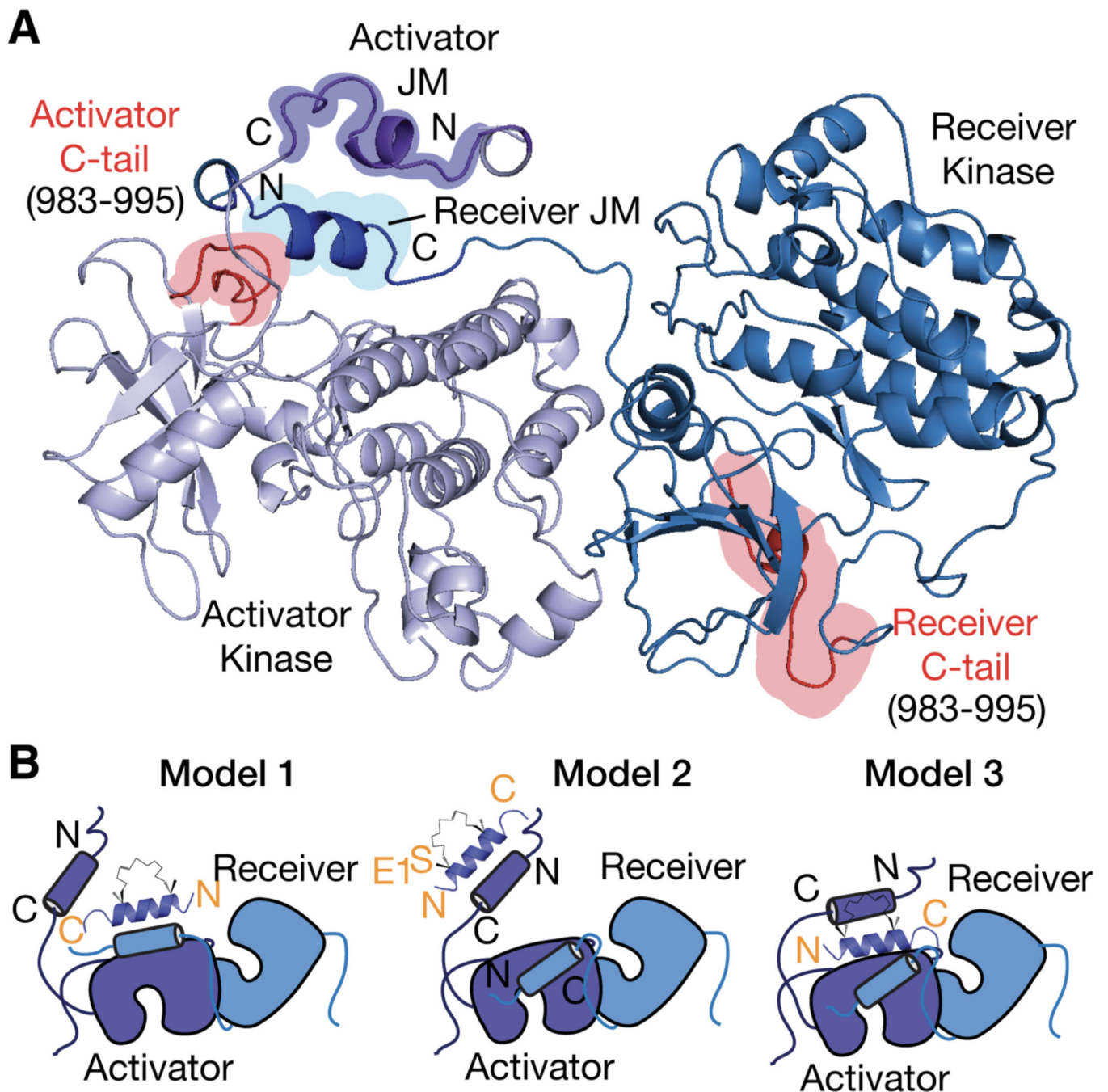
Figure 7.
Three models for the complex interactions between E1[S] and EGFR. (A) Molecular dynamics-derived model of the active EGF receptor asymmetric dimer [5]. Only residues 645–995 of the receptor are shown. The juxtamembrane (JM) segments (residues 650–666) of both the activator and receiver kinases are indicated, as are the JM latch of the receiver kinase and the C-terminal tail of the activator and receiver kinases (residues 983–995). (B) Cartoons illustrating three models for the interactions of E1[S] and EGFR. In Model 1, E1[S] binds to the EGFR JM segment of either the activator or receiver kinase (only the first of

these two options is shown) and inhibits its ability to pair with the JM segment of the second receptor of the dimeric partnership. In Model 2, $E1^S$ binds the JM segment of the receiver kinase as this segment interacts with the C-lobe of the activator kinase. In Model 3, $E1^S$ replaces the receiver JM segment from the C-lobe of the activator kinase and simultaneously interacts with the activator JM segment.